Botulinum Neurotoxin Inhibitor Binding Dynamics and Kinetics Relevant for Drug Design

*Kruti B. Patel[1,2], Olga Kononova[3,¶], Shuowei Cai[1], Valeri Barsegov[3], Virinder S. Parmar[2,4,#], Raj Kumar[2] and Bal Ram Singh[1,2,5 *]*

[1]Department of Chemistry and Biochemistry, University of Massachusetts Dartmouth, North Dartmouth, MA, USA
[2]Botulinum Research Center, Institute of Advanced Sciences, Dartmouth, MA, USA
[3]Department of Chemistry and Biochemistry, University of Massachusetts Lowell, Lowell, MA, USA
[4]Bioorganic Laboratory, Department of Chemistry, University of Delhi, Delhi, India
[5]Prime Bio Inc., Dartmouth, MA, USA

Present address:
[¶]Department of Materials Science and Engineering, University of California, Berkeley, Berkeley, CA, USA
[#]Department of Chemistry and Environmental Science, Medgar Evers College, The City University of New York, Brooklyn, NY, USA

KEYWORDS: Nitrophenyl Psoralen, Botulinum Neurotoxin Type A, Enzyme Kinetics, Isothermal Calorimeter, Molecular Dynamic Simulation, Graphics Processing Units, Drug Discovery, Ligand Binding Interactions

Abstract

Background: A natural product analog, 3-(4-nitrophenyl)-7*H*-furo[3,2-g]chromen-7-one, which is a nitrophenyl psoralen (NPP) was found to be an effective inhibitor of botulinum neurotoxin type A (BoNT/A).

Methods: In this work, we performed enzyme inhibition kinetics and employed biochemical techniques such as isothermal calorimetry (ITC) and fluorescence spectroscopy as well as molecular modeling to examine the kinetics and binding mechanism of NPP inhibitor with BoNT/A LC.

Results: Studies of inhibition mechanism and binding dynamics of NPP to BoNT/A light chain (BoNT/A LC) showed that NPP is a mixed type inhibitor for the zinc endopeptidase activity, implying that at least part of the inhibitor-enzyme binding site may be different from the substrate-enzyme binding site. By using biochemical techniques, we demonstrated NPP forms a stable complex with BoNT/A LC. These observations were confirmed by Molecular Dynamics (MD) simulation, which demonstrates that NPP binds to the site near the active site.

Conclusion: The NPP binding interferes with BoNT/A LC binding to the SNAP-25, hence, inhibits its cleavage. Based on these results, we propose a modified strategy for designing a molecule to enhance the efficiency of the inhibition against the neurotoxic effect of BoNT.

General Significance: Insights into the interactions of NPP with BoNT/A LC using biochemical and computational approaches will aid in the future development of effective countermeasures and better pharmacological strategies against botulism.

Introduction

Botulinum neurotoxin (BoNT) is designated as a "Category A" biothreat agent on the NIAID-priority-pathogen list. According to the United States Center of Disease Control and prevention, it poses a significant threat to public health. BoNTs are produced by anaerobic *Clostridium botulinum* and are the cause of botulism, a life-threatening neuroparalytic disease. BoNTs are the most toxic substances known to human beings and are incredibly potent food poisons, with a mouse LD_{50} of 0.1 ng/kg for type A (1, 2). Due to their high toxicity and relatively easy production, BoNTs create maximum fear among populations concerned with bioterror agents (3, 4). On the other hand, Botulinum toxin injections have also become one of the most popular cosmetic procedures worldwide because of their quick and easy administration and relative affordability compared to other more invasive cosmetic interventions (5).

Current therapy of botulism involves respiratory supportive care and administration of antitoxin. The only antitoxins available are equine antitoxin and the BabyBIG®, which is derived from the blood of human donors vaccinated with a pentavalent (ABCDE) toxoid vaccine, for infant botulism only. The treatment window for using antitoxin is short, and once symptoms develop, the antitoxin is not effective, since it cannot penetrate nerve cells. The muscle paralysis caused by BoNTs lasts for several months (1, 3, 6, 7) in part because of the long-lasting activity of the BoNT protease inside the cells, and patients require ventilator breathing support for months (6, 8). A bioterror attack can create a public health crisis due to ineffective therapy for prophylaxis and treatment.

Classically, there are seven known serotypes of BoNT, designated as A to G, among which types A, B, E, and F cause human botulism, with type A being the most potent serotype (2, 9, 10). BoNTs are 150 kDa proteins consisting of two chains linked through a disulfide bond.

The heavy chain (HC, 100 kDa) plays an accessory role by binding to the target nerve cells (through its C-terminus) and translocating the LC into the cell cytoplasm (through its N-terminus) (11). The light chains (LCs, 50 kDa) are zinc-endopeptidases (Fig. 1a), which cleave one or more soluble N-ethylmalemide sensitive factor attachment receptor (SNARE) proteins complex (Fig. 1b) (12). The BoNT/A LC exclusively cleaves neuronal protein SNAP-25, which is part of a SNARE complex responsible for synaptic vesicles to release acetylcholine into neuromuscular junctions. A lack of functional SNAP-25 completely inhibits acetylcholine-mediated signal transduction to skeletal muscle, resulting in flaccid muscle paralysis. The small molecule inhibitors (SMIs) have been identified against BoNT/A LC (13-16) since the enzyme can remain active in a neuron for several months in the absence of an antidote. SMIs such as captopril, thiorphan, phosphoramidon, and some natural product based inhibitors such as D-chicoric acid and lomofungin (17-19). On the other side, Zn-metal chelators such as hydroxamates and quinolinols are proven to be potent inhibitors (20-22). However, some reported quinolinol and hydroxymate inhibitors were either non-specific or toxic (21, 23-25).

In general, natural products are the source of the most diverse group of structures and have lower toxicity most of the time. By high-throughput screening of a library containing 300 natural compounds and their analogues acquired from the University of Delhi. A natural product-based inhibitor, 3-(4-nitrophenyl)-7H-furo[3,2-g]chromen-7-one, a nitrophenyl psoralen (NPP) (Fig. 1d) has been identified in our previous work, using biochemical assays, cellular assay, and in mouse phrenic nerve-hemidiaphragm preparations, and it has very low toxicity (>90% survival at 310 μM concentration) to neuroblastoma cells (26). Based on the potency of the natural analog NPP has been proven to be an efficient antidote with the ability to mitigate the

paralytic actions of BoNT (26). NPP displayed effective inhibition of catalytic action of LC proved by IC_{50} values as low as 4.74 ± 0.03 µM in *vitro* and 12.2 ± 1.7µM *ex vivo* (26).

In the current study, we have investigated the mechanism of interaction of NPP with its enzymatic target, BoNT/A LC, using fluorescence spectroscopy, isothermal calorimetry (ITC), enzyme kinetics, and molecular dynamics (MD) simulations. The mechanism of binding and inhibition of the catalytic domain of BoNT/A by NPP led to three major interpretations; a) NPP exhibits a mixed-type inhibition mechanism, b) binding of NPP to the BoNT/A LC is a spontaneous process with a significantly strong affinity (K_D =1.3 µM), and c) the NPP binds to the enzyme at the site near the hydrophobic pocket of the active site, thereby preventing a substrate from reaching the active site.

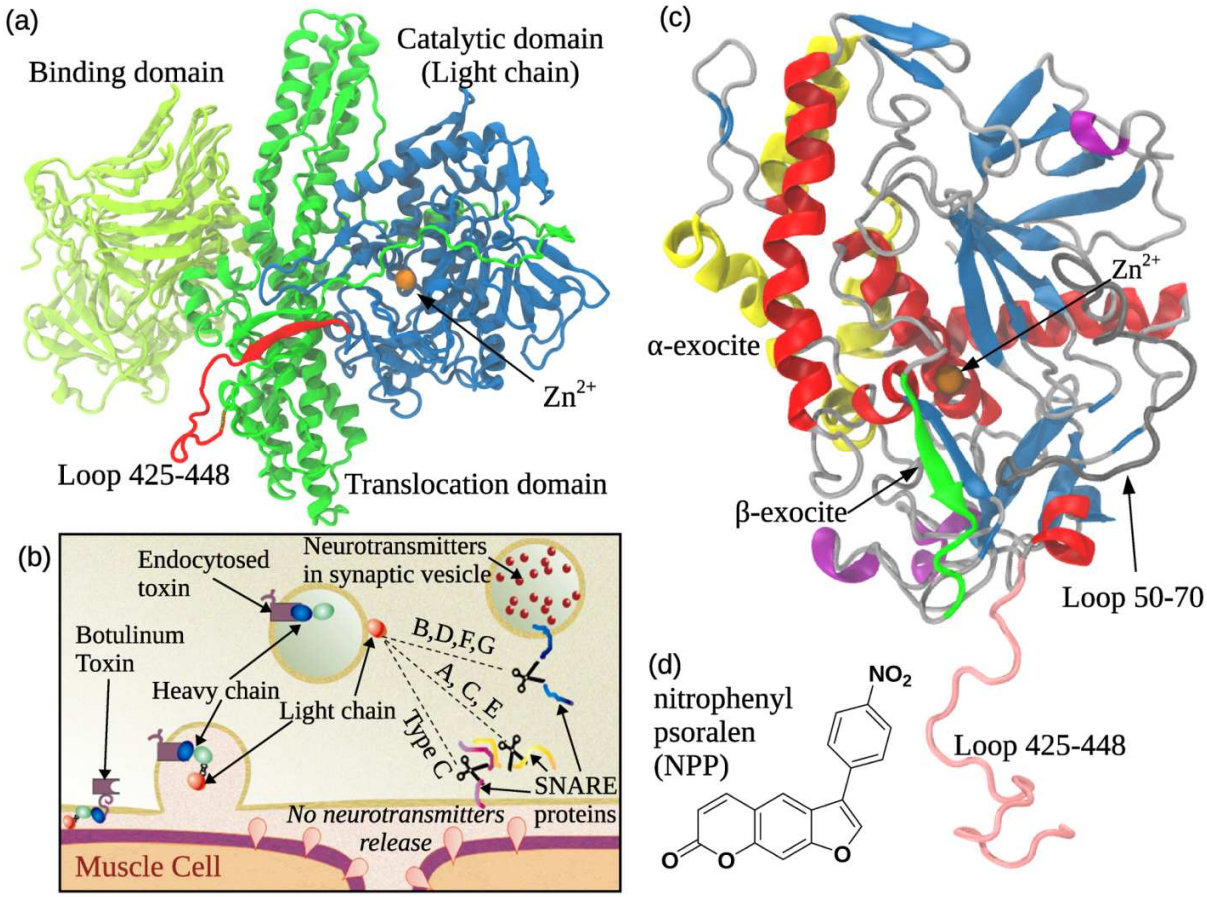

Figure 1. *Panel a: Structural representation of BoNT/A complex with ligand-binding domain (lime), translocation domain (green), and the catalytic domain (light chain; blue) (red). Reconstructed loop 425-448 is shown in red. The orange sphere denotes the position of* Zn^{2+}*-ion in the active site. Panel b: Schematic representation of infection mechanism by BoNT/A molecule: binding of the toxin to the cell, endocytosis, light chain release, and cleavage of the SNARE proteins to prevent fusion of synaptic vesicle, thus blocking neurotransmitters release leading to cell paralysis. The binding domain, translocation domain, and light chain of BoNT are shown as corresponding blue, green and red ovals. SNARE proteins synaptobrevin, SNAP-25, and syntaxin are shown as blue, yellow, and purple ribbons, respectively. Panel c: Cartoon representation of BoNT/A light chain (BoNT/A LC) showing elements of the secondary structure: α-helices (red), β-sheets (blue),* 3_{10}*-helices (purple), and random coil and turns (light gray). Also shown are important functional elements: α-exosite (yellow), β-exosite (green), C-terminal loop 425-448 (pink), loop 50-70 next to the active site (dark gray). Panel d: 3-(4-Nitrophenyl)-7H-furo[3,2-g]chromen-7-one, nitrophenyl psoralen (NPP) molecule. The size of the NPP is not to scale.*

Materials and methods

Recombinant BoNT/A LC

Recombinant BoNT/A LC was purified as reported by us earlier (27). The concentration of BoNT/A LC was determined using an extinction coefficient of 0.83 mg ml^{-1} cm^{-1} at 280 nm. Purity and catalytic efficiency of the enzyme were tested using SDS-PAGE (Sodium Dodecyl Sulphate – Poly Acrylamide Gel Electrophoresis) (Supplement Fig 1) and endopeptidase assay with peptide substrate, respectively (26).

Enzyme Kinetics

Enzyme kinetics was determined using the peptide-based substrate and procedure outlined above and published previously (13, 28). The assay conditions were the same as for the high-

throughput screening (HTS) assay as reported earlier (26). 50 nM of BoNT/A LC and concentration range from 5 to 25 μM of a peptide substrate was used for enzyme activity. The reactions were carried out at 25 °C, monitoring fluorescence in the first 10 min to calculate the initial reaction velocity. The fluorescence signals observed were within the linear range for the substrate concentrations chosen above. The concentrations of inhibitor used were chosen near its IC_{50} values. All the results shown were averaged over three independent measurements. The inhibition constants were measured indirectly by observing the enzyme activity under different inhibitor and substrate concentrations using modified Michaelis - Menten equation, $V_o = [Vmax(S)] / [(\alpha K_M) + (\alpha'(S))]$, where Vmax is the maximum rate of reaction, (S) is the substrate concentration, K_M is the Michaelis constant. The inhibitor dissociation constants *Ki* and *Ki'* of the enzyme and the enzyme-substrate complex were determined by modified factors α and α′, respectively, where $\alpha = 1 + [[I]/Ki]$ and $\alpha' = 1 + [[I]/Ki']$ and [I] is the inhibitor concentration. The inhibitor constants were estimated using the nonlinear regression method (29).

Structural Analysis of BoNT/A LC upon binding with inhibitor using fluorescence spectroscopy

Fluorescence measurements of BoNT/A LC (2 μM) at different concentrations of the inhibitor NPP (20 to 200 μM) were measured at two different temperatures (298.15 K and 310.15 K) using ISS K2 Fluorimeter (Champaign, IL, USA). Protein solutions (0.1 mg/ml) were excited at 295 nm. Emission spectra were recorded between 310 and 400 nm. Experiments were carried out in a 10 mm fluorescence cuvette. Excitation and emission slit widths were set at 4 nm. A small aromatic molecule can absorb the spectra in the range of 310 to 400 nm due to the inner filter

effect and re-absorption of NPP arising from UV absorption. The fluorescence data were corrected using the following equation (30).

$$F_{corrected} = F_{observed} \times 10^{\left(\frac{OD\ excitation+OD\ emmission}{2}\right)} \quad \text{(eq. 1)}$$

Where OD excitation and OD emission are the absorbances of NPP at 295 nm excitation and 324 nm emission wavelengths.

The quenching data were analyzed in terms of the Stern-Volmer equation.

$$\frac{F0}{F} = 1 + Ksv\,[Q] = 1 + Kq\ \tau o\ [Q]\ (eq.2)$$

Where F_0 and F are the intensity of BoNT/A LC in the absence of NPP and present of NPP at $[Q]$ concentration, K_{sv} is the Stern-Volmer quenching constant, K_q is the quenching rate constant and τo is the lifetime of the BoNT/A LC without the NPP.

The number of binding sites of NPP on BoNT/A LC was calculated using the following equation 3.

$$\log\frac{F0-F}{F} = n\log Ka - n\log\frac{1}{[Qt]-\frac{(F0-F)[Pt]}{F0}}\,(eq.3)$$

Where $[Qt]$ and $[Pt]$ are the concentration of quencher NPP and protein BoNT/A LC respectively. K_a represents the binding constant and n represents the number of the binding sites of NPP on BoNT/A LC.

The thermodynamic parameters such as enthalpy (ΔH) and entropy (ΔS) change can be calculated using Van's Hoff equation.

$$ln\,K = -\frac{\Delta H}{RT} + \frac{\Delta S}{R}\ (eq.4)$$

Where *K* is the binding constant at temperature *T*.

The free energy change ΔG is estimated from the eq. 5.

$$\Delta G = \Delta H - T\Delta S\ (eq.5)$$

Binding studies of BoNT/A LC and NPP by isothermal titration calorimetry (ITC)

Purified BoNT/A LC was subjected to a final gel filtration step using Bio-Rad mini spin size exclusion spin columns (Bio-Rad, California, MA) to ensure a complete buffer exchange, as well as to exclude trace amounts of auto cleavage products. All experiments were carried out in the same buffer to control for the heat of dilution effects, i.e. 10 mM HEPES (pH 7.4) supplemented with 150 mM NaCl and surfactant 0.5% p-20. The protein concentrations were confirmed by UV-visible absorbance measurements. Calorimetric titration was performed three times on a TA instrument -ITC calorimeter (NANO ITC from TA Instruments, New Castle, DE, USA) at 298 K. BoNT/A LC was used at a concentration of 40 µM in the cell, and inhibitor NPP at a concentration of 400 µM in the injection syringe. Before the titration, the samples were degassed for 10 min. The positive deflections observed at the end of the titration reflected the enthalpy of dilution of the inhibitor solution and were subtracted from the binding data. The analysis of the data was done with NanoAnalyze Software 2.2.4 (TA Instruments) using an independent sites model setup to obtain the following parameters: the number of binding sites (*N*), binding enthalpy (ΔH), and binding constant (K_D). The free energy change was calculated using equation 5. The first injection systematically showed a decreased enthalpy due to the technical limitations of the instrument and was omitted from curve fitting.

Molecular Dynamics

Atomic structural model of BoNT/A LC

The BoNT/A LC molecule spans amino acids Met1 to Lys448 (Fig. 1 a, c). However, to date, all available atomic structures of the BoNT/A LC are incomplete, missing the C-terminal loop (amino acids Phe425 – Lys448; Fig. 1c). To reconstruct the BoNT/A LC with the C-terminal part (PDB https://doi.org/10.6084/m9.figshare.11954460), we started from the structure of the entire BoNT/A molecule available in the Protein Data Base (PDB code 3BTA (11); Fig. 1a). The missing C-terminal loop (amino acids Phe425 – Lys448) was first reconstructed using VMD Molefacture Plugin (31) using the amino acid sequence given in the PDB structure 3BTA. Then, this sequence was attached to the BoNT/A molecule (Fig. 1a), and the obtained structure was energy-minimized during 10^6 steps while keeping the rest of the molecule fixed. Next, the entire molecule with the reconstructed C-terminal loop was energy-minimized during 10^6 steps, heated up to 300K, and equilibrated at a constant temperature for 10 ns. Lastly, the BoNT/A LC portion (amino acids Met1 – Lys448) including Zn^{2+}-ion was truncated from BoNT/A molecule, additionally equilibrated for 10 ns, and used in all subsequent ligand-binding simulations (Fig. 1c).

The *in silico* models of BoNT/A and BoNT/A LC were constructed using the CHARMM force field (32). Energy minimization, heating, and equilibration were carried out using the all-atom MD simulation in the implicit solvent with the Solvent Accessible Surface Area (SASA) model of water (33) accelerated on Graphics Processing Units (GPUs) (34). Energy minimization was performed using the steepest descent algorithm. Heating and equilibration were performed with simulation time step 1 fs, using damping coefficient γ= 50.0 ps^{-1}, which corresponds to ambient water viscosity. The reconstituted structural models of BoNT/A light chain is public available on figshare: https://doi.org/10.6084/m9.figshare.11954460

Atomic structural model of nitrophenyl psoralen (NPP)

The all-atomic structure of NPP (Fig. 1d, *inset* in Fig. 1c) was obtained using the Spartan software tool V.2.0.7. The molecular topology and parameterization of the model were prepared using *antechamber* utility of AMBER Tools package (35) with the general AMBER force field (GAFF) (36, 37). The structure was solvated in water using the TIP3P water model and the size of the water box 35Å×37Å×31Å. The obtained model was energy-minimized for 10^6 steps, heated, and equilibrated for 1 ns using AMBER software implemented on GPUs (38, 39). The simulation time step was 2 fs, and the conditions of constant temperature and pressure were maintained by using weak-coupling rescaling and Berendsen barostat.

Model systems

We performed simulations of one NPP molecule binding to BoNT/A LC as a model. The LC/A was placed in the center of the water box and the NPP molecule was assigned with a random position around LC. The system was solvated in water using the TIP3P water model with the addition of counter ions to neutralize the systems' total charge. Parameters of solvation are provided in supplement Table S1. The models' preparation and binding simulations were performed using the AMBER MD package. Energy minimization of the model system was carried out during 10^6 steps, heating and equilibration were performed for 10 ns, with the time step 2 fs. For the equilibrium production runs, we applied weak-coupling rescaling and Berendsen barostat to maintain constant temperature and pressure, and we used periodic boundary conditions. The simulations were carried out using GPU accelerated implementation of AMBER MD package (38, 39) on GeForce GTX780 graphic cards. The durations of independent simulation runs are given in supplement Table S1.

Data availability

A description of the data: Complete PDB structure of the BoNT/A LC with reconstructed C-terminal part and non-bound nitrophenyl psoralen (NPP) molecule. PDB of BoNT/A LC structure was reconstructed from PDB entry 3BTA by using MD simulations accelerated on GPUs. The name(s) of the repository(ies)- Figshare at- https://figshare.com/articles/Botulinum_Neurotoxin_A_Light_Chain_and_Psoralen_molecule/11954460

Digital object identifiers (DOIs) - https://doi.org/10.6084/m9.figshare.11954460

Results and Discussion

Enzyme Kinetics

To explore the mechanism of BoNT/A LC inhibition by NPP, the Michaelis-Menten enzyme inhibition kinetics model was used. The Lineweaver-Burk plot was constructed for BoNT/A LC endopeptidase activity against different concentrations of the peptide substrate in the presence and absence of NPP at different concentrations. In the absence of the inhibitor, K_M was estimated to be 18.4 ± 1.8 μM, which is similar to the value from our previously reported studies (13, 28) From the Lineweaver-Burk plot (the double- reciprocal plot) of enzyme kinetics is generated by plotting $1/v$ as a function of $1/[s]$ (Fig.2), it can be concluded that the NPP showed a mixed type (competitive and uncompetitive) of inhibition, suggesting that the inhibitor binds to both free enzyme and enzyme-substrate complex. The inhibitor constant *Ki* defines the binding of inhibitor with the enzyme (i.e. $Ki = ([E][I]) / [EI];$ where $[E],[I]$ and $[EI]$ are enzyme, inhibitor, and enzyme-inhibitor complex concentrations, respectively), whereas *Ki'* defines the binding of the

inhibitor with the enzyme-substrate complex (i.e. *Ki'= ([ES][I])/[ESI];* where *[ES],[I]and [ESI]* are enzyme-substrate complex, inhibitor, and enzyme-substrate-inhibitor complex concentrations, respectively). The *Ki* and *Ki'* were estimated to be 5.8 ± 0.7 μM and 11.5 ± 2.9 μM, respectively. Because $K_i \neq K_i'$, the inhibitor binds both to BoNT/A LC and to BoNT/A LC - SNAP-25 complex with different affinities. Moreover, the data showed both $K_i < K_i'$ and a linear increase in K_M values (apparent K_M (K_M^{app},) 19.4, 20.5 and 21.9 μM) with an increase in the inhibitor concentration (3, 6, and 12 μM, respectively) (Table 1), thus indicating that NPP has high probability to bind to free BoNT/A LC rather than to the BoNT/A LC - SNAP-25 complex. The plots of *1/v* against [NPP] (Dixon plot) and of *[s]/v* against [NPP] (Cornish-Bowden plot) confirmed the mixed-type inhibition of BoNT/A LC by NPP (39). Since the Dixon plot does not distinguish between competitive and mixed-type inhibition kinetics, the Cornish-Bowden plot was used to determine the mode of inhibition. The Cornish Bowden plot indicates the data for each substrate concentration falls on a straight line that intersects at I =- K_i' for the mixed inhibition, whereas the lines are parallel for the competitive inhibition. The Cornish-Bowden plots indicated mixed inhibition. The graphical analysis of converging point in the Dixon plot provides a measure of K_i (5.8 μM), (Supplement Fig 2a), whereas the Cornish-Bowden plot provides a measure of K_i' (10.8 μM) (Supplement Fig 2b) which are consistent with the K_i and K_i' values (5.9 and 11.5 μM, respectively) obtained from the double reciprocal plot as indicated above.

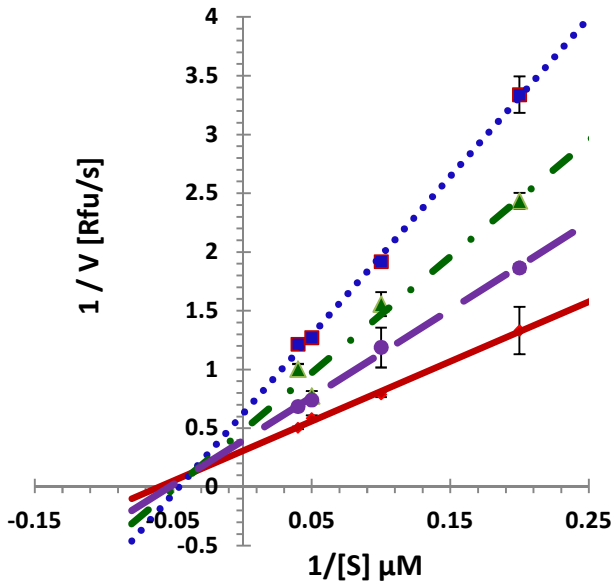

Figure 2. *The double-reciprocal plot (Lineweaver-Burk plot) of substrate concentration versus velocity. The initial rates kinetics were determined by incubating BoNT/A LC (50nM) at various concentration of the peptide substrates ([s] = 5, 10, 20, 25 µM) and ([I] = 0 µM (red, solid), 3 µM (purple, long dash), 6 µM (green, dash) and 12 µM (blue, round dot). The Lineweaver-Burk plot data is described as a mixed inhibition mode. The characteristic of mix inhibition mode such that* K_M *(negative reciprocal of x-intercept) is increasing, and maximum velocity Vmax is decreasing with inhibitor concentration. The values of the kinetic constants* K_M *and* V_{max} *are summarized in Table 1. Each data point represents the mean with an error bar of the three independent experiments.*

Table 1. Kinetic constants (average and standard deviation) of the BoNT/A LC catalyzed reaction in the presence and absence of NPP. The K_M and V_{max} values were determined by a nonlinear regression method. [c], NPP concentration.

NPP [c]	V_{max} (RFU/s)	K_M (μM)
0 μM	3.44 ±0.11	18.37 ±1.88
3 μM	2.13 ±0.06	19.41 ±2.05
6 μM	2.09 ±0.01	20.45 ±0.32
12 μM	1.56 ±0.15	21.91 ±3.61

** Data represent the averages from three independent experiments (mean ± SD, n=3).*

Binding Analysis of BoNT/A LC and NPP

Steady-state Fluorescence measurements

Conformational changes in BoNT/A LC upon binding with inhibitor were further examined at the tertiary structure level by monitoring intrinsic tryptophan fluorescence in the presence and absence of NPP. Different concentrations of NPP were incubated with 2 μM of BoNT/A LC. Since the NPP was prepared in DMSO, BoNT/A LC incubated with DMSO was used as a control. Fig. 3 shows the similar fluorescence intensity of BoNT/A LC in the absence (red line) and in the presence (green dotted line) of DMSO. Since 280 nm is the wavelength at which tryptophan and tyrosine residues absorb maximally, the excitation at 295 nm was chosen to selectively excite Trp residues, avoiding contribution from Tyr fluorescence. Emission λ_{max} was observed at 324 nm (Fig. 3), indicating that Trp residues in BoNT/A LC are buried and constrained in a hydrophobic environment (40, 41). The emission λ_{max} upon excitation at 295 nm for BoNT/A LC treated with NPP was also observed at 324 nm (Fig. 3).

Additionally, the quenching of Trp fluorescence of BoNT/A LC was dependent on NPP concentration. Notably, when BoNT/A LC was incubated with DMSO, no reduction of the signal was observed, suggesting that the resulted signal quenching is due to the presence of NPP. The fluorescence spectroscopy results showed that NPP quenched intrinsic fluorescence of BoNT/A LC. The corrected intensity of the Trp fluorescence signal at λ_{max} of BoNT/A LC in the presence of 20, 50, 100, and 200 µM concentrations of NPP showed a reduction of the signal to 88, 84, 73, and 59 %, respectively (Supplement Fig S3), suggesting NPP can form a complex with BoNT/A LC, hence contributing in the quenching of intrinsic fluorescence of BoNT/A LC.

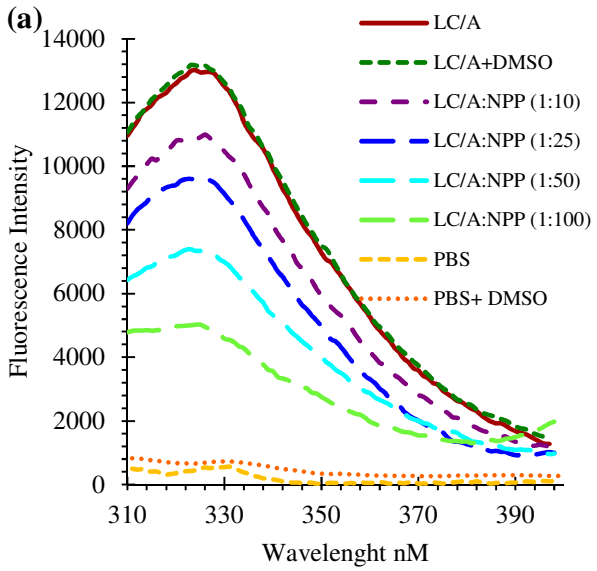

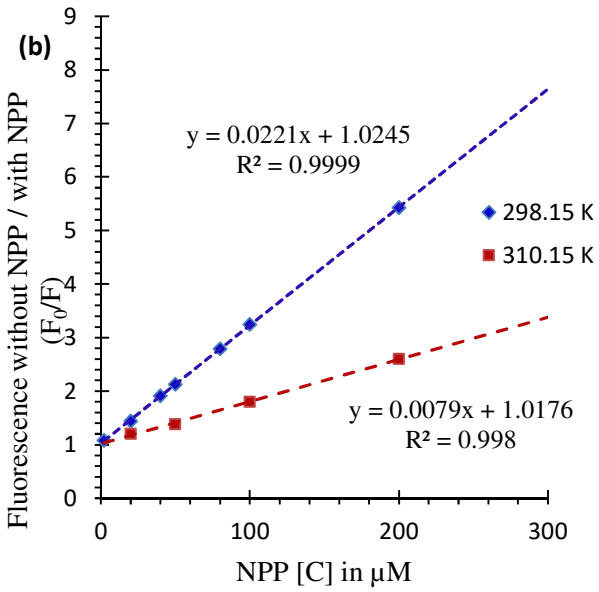

Figure 3. *Effect of NPP on the intrinsic fluorescence of BoNT/A LC with an excitation wavelength of 295 nm. Panel a: The fluorescence intensity at emission maxima showing the drop in intrinsic fluorescence intensity of BoNT/A LC (2 µM) corresponding to the concentration-dependent addition of NPP in the ratio of 1:10, 1:25, 1:50, 1:100. The intrinsic fluorescence of BoNT/A LC remains unchanged in the presence of DMSO. Panel b: The Stern-Volmer plot of the fluorescence intensities in the absence and presence of NPP quencher (F_0/F) versus NPP concentration in M at 298.15 K and 310.15 K temperature.*

The fluorescence quenching of BoNT/A LC by NPP could be due to energy transfer, complex formation, molecular rearrangements, and collision between fluorophores. There are two modes of fluorescence quenching: static quenching and dynamic quenching. Static and dynamic quenching can be distinguished by the different temperature dependencies shown by the Stern-Volmer plot. The Stern-Volmer plots of the fluorescence intensity of BoNT/A LC without and with NPP (F_0/F) vs. different concentrations of NPP at 298 K and 310 K temperature are

linear (Fig 3b). Furthermore, the K_{sv} at 25 ºC and 37 ºC are 22.10 x 10^3 M^{-1} and 7.90 x 10^3 M^{-1}, respectively (Table 2). Both above observations suggested that the quenching of BoNT/A LC fluorescence by NPP is a static quenching. Therefore, we can conclude that BoNT/A LC-NPP complex formation occurs through a strong coupling regime. (30). Furthermore, the quenching rate constant K_q (calculated using eq. 2) at 298K and 310K is 1.03 X 10^{13} $M^{-1}S^{-1}$ and 0.36 X 10^{13} $M^{-1}.S^{-1}$, respectively (eq. 2) for BoNT/A LC life-time τ_0 2.12 X 10^{-9} s (41). The derived K_q was much higher than the maximum scattering collision quenching rate constant of various quenchers of fluorescence moieties in biopolymer (2.0 X 10^{10} $M^{-1}.S^{-1}$) (42), suggesting that BoNT/A LC - NPP interaction follow the static quenching mechanism rather than the dynamic collision quenching.

Number of NPP binding site

The study of inhibitor protein interaction can provide insight into the binding ability and stability of the inhibitor-protein complex. The binding of NPP to BoNT/A LC was determined from the fluorescence intensity data using equation 3 (Materials and Methods). The number of binding sites *n* and binding constant K_a of NPP-BoNT/A LC interaction can be calculated using the plot of log $(F_0\text{-}F)/F$ vs. log $(1/([Q_t]\text{-}(F_0\text{-}F)[P_t]/F_0)$ (equation 3). The value of *n* for NPP binding with BoNT/A LC is approximately 1. The binding constant K_a (26.3 x 10^3M^{-1} and 8.7 x 10^3M^{-1}) decreases with the temperature increasing from 298 K to 310 K, indicating that the stability of the BoNT/A LC – NPP complex reduces at higher temperature (Table 2). The dissociation constant (inverse of K_a) of NPP can be calculated as 38 µM at 298K.

Thermodynamic Analysis of the Fluorescence data

The interaction of NPP binding to BoNT/A LC involves four major forces i.e. hydrophobic interactions, hydrogen bonding, van der Waals forces, and electrostatic forces. The thermodynamic parameters ΔH and ΔS were calculated by the van't Hoff plot (ln K vs 1/T) and are presented in Table 2. The negative ΔH (-70.80 kJ.mol^{-1}) indicates the NPP-BoNT/A LC binding process is exothermic, which is also consistent with decreasing K_a value as the temperature is increasing. The data suggested negative ΔH and ΔS values (Table 2) indicating that hydrogen bonds and van der Waals forces played major role in the binding of NPP to BoNT/A LC.

Table 2. The quenching constants (K_{sv}), binding constants (K_a), number of binding sites (n), and relative thermodynamic parameters of NPP-BoNT/A interaction using fluorescence spectroscopy.

T (K)	K_{sv} (x10^3 M^{-1})	R^{2a}	K_a (x10^{3}M^{-1})	n	R^{2b}	ΔH (kJ. mol^{-1})	ΔS (kJ.mol^{-1} K^{-1})	ΔG (kJ. mol^{-1})
298	22.1	0.98	26.3	0.9	0.99	-70.8	-0.15	-25.2
310	7.9	0.99	8.7	0.9	0.99	-70.8	-0.15	-23.4

R^{2a} and R^{2b} are the regression coefficients for K_{sv} and K_a values respectively.

Isothermal calorimetry (ITC) Analysis

To understand NPP's interaction with the BoNT/A LC, ITC experiments were carried out to directly determine the stoichiometry, entropy, enthalpy, and association constant. The binding

stoichiometry (n) of NPP to BoNT/A LC is 2.8 (Fig. 4). This value indicates that ligand binds on 2-3 sites on the enzyme surface. In other words, either BoNT/A possesses multiple binding sites for NPP or multiple NPP molecules bind to the same site with the similar affinity. The data is also consistent with the mixed-type inhibition kinetics we observed for this inhibitor (Fig. 2). Further analysis of ITC data allowed us to calculate thermodynamic parameters. We found that ΔS = 0.08 kJMol^{-1}K^{-1}, ΔH = -10 kJMol^{-1} (Fig. 4). Higher negative enthalpy means the binding affinity of NPP to BoNT/A LC is strong which is substantiated by higher K_D ~ 1.3 µM (Fig 4). The Gibbs free energy change ΔG was calculated using eq. 5 to be -34.5 kJ.mol^{-1}. The similar negative Gibbs free energy change was calculated by fluorescence data (-25 kJ.mol^{-1}) inferred that the NPP bind to BoNT/A LC is a spontaneous process. The positive entropy value indicated that the system becomes more disordered upon binding (Fig. 4). To further investigate this possibility, we carried out MD simulations of NPP binding to BoNT/A LC (see results below).

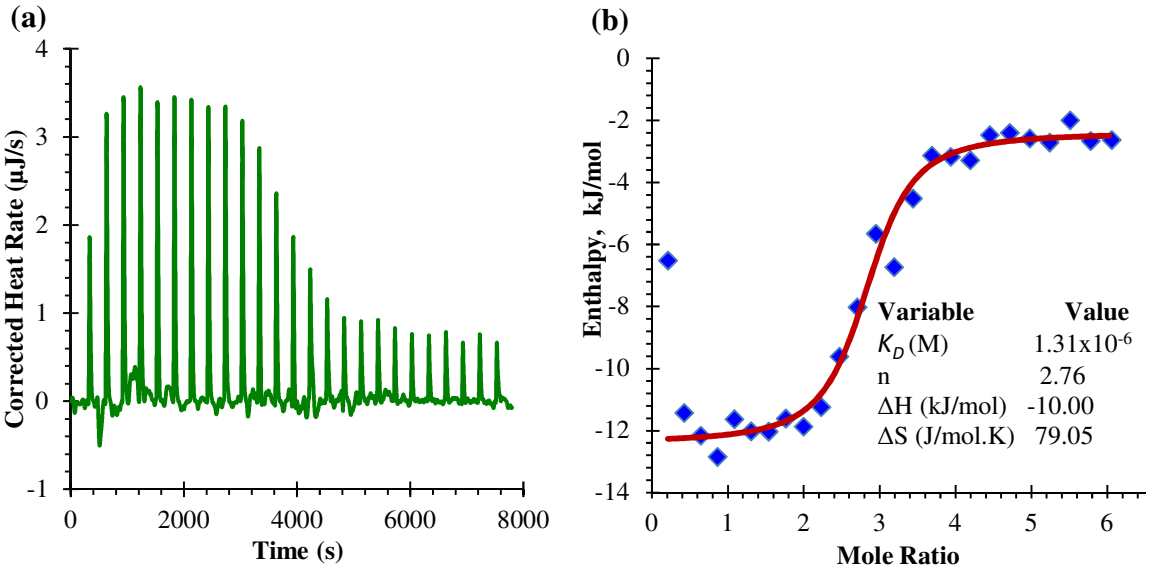

Figure 4. *Isothermal titration calorimetry of NPP interacting with BoNT/A LC. Panel a: Raw data obtained for 25 injections of 10µl of 0.4 mM NPP solution into the sample cell containing 40 µM BoNT/A LC (after subtraction of the integration baseline.) Panel b: Normalized integrated enthalpies plotted against the molar ratio of inhibitor NPP to BoNT/A LC.*

Molecular Dynamics simulations

Equilibrium simulations of BoNT/A LC with NPP molecule

To explore the binding mechanism of NPP to BoNT/A LC, we carried out a 1 µs-long equilibrium simulation (see Materials and Methods). To monitor the binding transitions, we analyzed the dynamics of the total number of binary contacts between the atoms forming NPP molecule (see Fig. 1) and amino acids side chains of BoNT/A LC. The molecules are said to form a binary contact if a distance between the center of mass of any amino acid side chain of BoNT/A LC and any atom of the NPP molecule is less than 15 Å and it persists for 5 ns. The curves of the total number of binary contacts vs. time are displayed in Fig. 5.

Analysis of binary contacts shows that the binding of NPP proceeds in three stages (Fig. 5). The first stage lasts up to ~ 50 ns of the trajectory, and it represents the initial interaction between loop 50-70 of the BoNT/A LC and NPP molecule (Fig. 5, snapshots 1a and 1b). Detailed analysis of binding contacts revealed that the initial binding occurs due to hydrophobic interactions of NPP with aliphatic residues Leu59, Pro61, Pro62, Pro63 of BoNT/A LC, polar interaction with hydrophilic residues Asn53, Asn60, Tyr73, Ser75, and electrostatic interactions with charged residues Glu55, Glu56, Glu64, Lys66 (Table 3). During the second stage, NPP moves towards the active site of the BoNT/A LC (Fig. 5, snapshots 2a, 2b). Interestingly, we

found that loop 50-70 facilitates the binding of NPP by tilting inwards and outwards, thus preventing the inhibitor from unbinding while it adjusts itself in the active site (Movie S1).

NPP molecule adapts unique orientation in the active site, with a three-ring psoralen moiety, placed perpendicular to the direction of the LC groove and substrate binding site, while the nitrophenyl residue rotates ~ 90° relative to the psoralen moiety, and creates stable contact with loop 50-70. This conformation emerges due to hydrophobic interaction of NPP with residues Pro62, Ala65, Val68, Pro239, Ala158, Val258, polar interactions with residues Asn53, Ser71, Tyr73, Ser157, Gln162, Asn240, Ser259, and electrostatic interactions with residues Glu56, Lys66, Asp159, Glu164, Lys166, Arg187, Glu257, Glu262, with all interactions persisting for ~0.15 μs. It is important to note that the stable contacts created by NPP with residues Glu257, Val258, and Ser259 perturb the secondary structure of the LC resulting in the transformation of β-strand Val242–Tyr250, forming the β-exosite, into a random coil (Fig. 5 snapshots 2a, 2b). The third stage of the binding starts after ~ 0.2 μs, NPP moves closer to Zn^{2+}-ion, thereby blocking the LC active site (Fig. 5, snapshots 3a, 3b) and creating additional hydrophobic contacts with residues Pro69, Asn238, and Val242 of BoNT/A LC (Table 3) (see Movie S1).

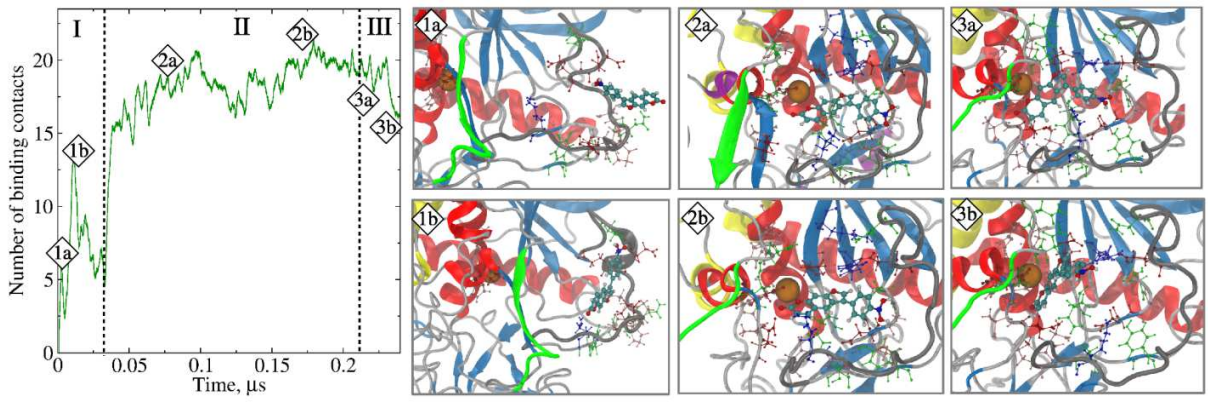

Figure 5. *Dynamics of binding interactions between NPP molecule and BoNT/A LC quantified using the total number of atomic binding contacts from 0.25 μs of equilibrium MD simulations. The initial binding event (stage I, snapshots 1a, 1b) is followed by the adjustment of NPP next to the active site of LC (stage II, snapshots 2a, b), and further movement toward Zn^{2+}-ion (stage III, snapshots 3a, 3b), which results in blocking of the active site. The structure of LC is shown in ribbon representation (color denotation is same as in Fig. 1); the NPP molecule is shown in thick balls-and-sticks representation (color denotation is same as in Fig. 1); the amino acid side chains of LC forming stable contacts with NPP are shown as thin balls-and-sticks.*

Table 3. List of BoNT/A LC amino-acid residues forming stable contacts with NPP molecule at various stages of the binding process (see also Fig. 5).

Stage	**Time (μs)**	**Amino acids**		
		Electrostatic	**Hydrophobic**	**Polar**
I	0 – 0.05	Glu55, Glu56, Glu64, Lys66	Leu59, Pro61, Pro62, Pro63	Asn53, Asn60, Tyr73, Ser75
II	0.05 – 0.20	Glu56, Lys66, Asp159, Glu164, Lys166, Arg187, Glu257, Glu262	Pro62, Ala65, Val68, Pro239, Ala158, Val258	Asn53, Ser71, Tyr73, Ser157, Gln162, Asn240, Ser259
III	0.20 – 0.25	Glu56, Lys66, Asp159, Glu164, Lys166, Arg187, Glu257, Glu262	Pro62, Pro69, Ala65, Val68, Pro239, Ala158, Val242, Val258	Asn53, Ser71, Tyr73, Ser157, Gln162, Asn238, Asn240, Ser259

Discussion:

In this study, we examined the mechanism of BoNT/A LC inhibition by NPP using several experimental techniques, such as enzyme kinetics, binding kinetics, spectroscopy, and equilibrium simulation using molecular dynamics to explore specific binding interactions at the level of atoms. Many BoNT inhibitors exhibiting competitive (43), non-competitive (28, 44), or mixed type (13) inhibition mechanisms have been reported in the literature. We found that NPP showed mixed-type inhibition, with characteristics that correspond to a competitive inhibition (higher K_M^{app} with increased inhibitor concentration; Fig 2). The nature of mixed-type inhibition by NPP indicates that the enzyme might possess a secondary binding site in addition to the active site, and the inhibitor might interfere with both the free enzyme and the enzyme-substrate complex. However, an affinity to the free enzyme is larger than to the enzyme-substrate complex. The crystal structure of SNAP-25 in the BoNT/A LC complex suggests the existence of two exosites (on the BoNT/A LC) involved in substrate binding (45). The α-exosite is located outside of the catalytic cleft of the enzyme, but is predicted to play a key role in the substrate specificity (45); the β-exosite protrudes into the enzyme's catalytic center, and also plays a key role in the substrate recognition and enzymatic activity (45). We determined that $K_i < K_i'$ indicating that the inhibitor's binding near the active site occurs with higher affinity, thus being a competitive inhibitor. We found that a fraction of NPP molecule binding occurs at the β-exosite located near the active site. β-exosite comprises of two β-strands (β-strand-I from Val242-Val245 and β-strand-II from Gly255-Ser259) connected through '250 loop' (46). Upon NPP binding at the β-exosite, the β-strands transformed into random coil indicating the structural change at the β-exosite (Fig 5, snapshots 2a, 2b and Movie S1). The observed structural changes at this region could interfere the SNAP-25 interaction to BoNT/A LC. This could be the possible

reason for the reduction of endopeptidase activity of BoNT/A LC in the presence of NPP and its non-competitive inhibition enzyme kinetics (26).

The fluorescence spectroscopy results showed that NPP quenched BoNT/A LC intrinsic fluorescence. NPP has aromatic rings in conjugation, which absorb at 230 to 350 nm that interfere with the LC's fluorescence signal in the presence of NPP due to the inner filter effect. The inner filter effect was nullified by correcting the emission intensity at λ_{max} of BoNT/A LC using eq. 1 (see Materials and Methods). Even after the correction of the inner filter effect, there was a significant effect of NPP on the BoNT/A LC fluorescence signal (about 12% change near K_i concentration), As a result of static quenching (decreasing slope with increasing temperature) (Fig. 3c) can also be concluded that BoNT/A LC-NPP complex formation occurs through a strong coupling (30).

The ITC obtained NPP's dissociation constant, K_D as 1.3 μM, and the thermodynamic parameters suggest that the binding is entropy-driven (Fig. 4). This observation is in agreement with the results reported by Burnett et al. (15), showing similar dissociation constant of 4.6 μM for NSC 240898 (with well-defined pharmacophore groups) and BoNT/A LC, (dissociation constant at 1:1 stoichiometry of inhibitor and LC). However, the obtained stoichiometry of NPP binding to BoNT/A LC is 3:1 as opposed to 1:1 for NSC 240898. Thus, ITC data supports our conclusion from the kinetic experiments that NPP binds favorably to BoNT/A LC. The Trp fluorescence spectroscopy identifies at least one of the binding sites near the fluorescent Trp 118 located near the BoNT/A LC active site (47) (Table 2). In the MD simulation, we observed that NPP molecules tend to aggregate, forming a stack structure of two-three molecules aligned in a parallel manner (Supplement Fig S4). The interactions occur when any two molecules approach each other at closer than ~1.0 nm distance. The stoichiometry of NPP to BoNT/A LC, 3:1 in the

ITC data might be the case of the multiple molecules combine to bind at one site. Hence, not only the dynamics of the BoNT/A enzyme but also the dynamics of small inhibitor molecules should be explored. Clearly, such a non-trivial dynamic behavior can significantly affect the efficiency of the inhibitor and should be carefully explored for potential drug development purposes.

To get insight into the binding mechanism and atomistic interactions between BoNT/A LC and NPP, we carried out MD simulation of the molecules binding. MD simulations is a powerful tool widely used for studying biological processes at the atomic level (48-51). In this work, we utilized the all-atom MD simulations to probe the mechanism of NPP inhibitor binding to BoNT/A LC. Analysis of MD simulation data revealed that loop 50-70 of BoNT/A LC plays important role in inhibitor binding. The loop 50-70 of the BoNT/A LC latches on the inhibitor molecule thus preventing its dissociation, and guides the inhibitor to the active site. The residue positions in the loop 50-70 are crucial for binding since it seems to play the role of a "doorkeeper" opening and closing the entrance to the BoNT/A LC active site. Hence, one of the strategies for drug development could be proposing an inhibitor, which could bind to the loop 50-70 with high affinity. Additionally, it is also important to note that in the case of NPP we observed β-exosite distortion due to new contacts that emerged between β-exosite and NPP (Table 3) (22, 52).

Previously, the mechanism of inhibition of BoNT/A LC by small molecules was examined using molecular docking approaches (52-54) and MD simulations (54, 55). Hu et al. (52) demonstrated that small inhibitors have high binding affinity to various sites on the LC surface, not only to the active site. Although a large number of longer simulations are required to thoroughly resolve the mechanisms of NPP binding to BoNT/A LC, to the best of our

knowledge, these are the first atomistic simulations of the inhibitor binding to BoNT/A, in which the full-length structure of BoNT/A LC has been used. These efforts have enabled us to explore the NPP inhibitor binding dynamics on the microsecond timescale and to follow the dynamics of enzyme-inhibitor interaction to resolve the association-dissociation transitions for BoNT/A LC enzyme and NPP inhibitor dynamics at the same time.

Conclusions

In conclusion, using a powerful combination of precise biochemical experiments, including enzyme inhibition kinetics, ITC, fluorescence spectroscopy, and computational molecular modeling; we explored the mechanism of inhibition and binding interactions of NPP ligand to BoNT/A LC enzyme. The experimental results have provided preliminary information for the interactions of the inhibitor molecule to the BoNT/A LC. These interactions are correlated with the loss of enzyme activity and can explain the mixed type of inhibition kinetics. The steady-state fluorescence analysis identified one of the NPP binding sites at BoNT/A LC. Although our data provide structural insight into the dynamics of drug-protein interactions, which can be used to uncover the mechanisms of BoNT/A LC inhibition by NPP ligand, further studies are needed to develop NPP into a therapeutic drug. Nevertheless, the combined experimental and computational studies undertaken in this work provide a novel platform to improve the therapeutic potency of NPP against BoNT/A intoxication.

ASSOCIATED CONTENT

Supporting Information

The supporting information is available free of charge on the BBA Publication website.

AUTHOR INFORMATION

Corresponding Authors

***E-mail:** bsingh@inads.org Phone: 508-992-2042

ORCID

Bal-Ram Singh : 0000-0002-9069-1487

Funding

This work was supported by the United State Department of Defense (DOD) consortium (W81XWH-14-C-0070), Maryada Foundation, Infinity Foundation and NSF (grant DMR 1505316 to VB).

Notes

The authors declare that there are no conflicts of interest.

ACKNOWLEDGMENTS

Authors would like to sincerely thank Dr. Charlene Mello from U.S. Natick Soldier Research lab for allowing us to use the ITC instrument. Authors appreciate Shashwat Malhotra from University of Delhi for his assistance.

ABBREVIATIONS

BoNT, Botulinum neurotoxin; HC, heavy chain; LC, light chain; SNARE, soluble N-ethylmalemide sensitive factor attachment receptor; SMIs, small molecule inhibitors; NPP, nitrophenyl psoralen; ITC, isothermal calorimetry; MD, molecular dynamics; SDS-PAGE, Sodium Dodecyl Sulphate – Poly Acrylamide Gel Electrophoresis; HTS, high-throughput

screening; K_M; Michaelis constant; V_{max}, maximum reaction rate; DMSO, dimethylsulfoxide; GPUs, Graphics Processing Units; ΔH , change of enthalpy; ΔS, change of entropy; SASA , Solvent Accessible Surface Area.

AUTHOR CONTRIBUTIONS:

B.R.S. conceived the idea and K.B.P. carried out the experiments, validate and analyzed the data. O.K. and V.B. carried out computational data and interpretation. V.P. shared inhibitor library. K.B.P., O.K. and B.R.S. wrote the original manuscript, review and editing. B.R.S. and V.B. aquried funding. S.C. and R.K. manuscript review and editing.

References

1. Arnon SS, Schechter R, Inglesby TV, Henderson DA, Bartlett JG, Ascher MS, Eitzen E, Fine AD, Hauer J, Layton M, Lillibridge S, Osterholm MT, O'Toole T, Parker G, Perl TM, Russell PK, Swerdlow DL, Tonat K. 2001. Botulinum toxin as a biological weapon: medical and public health management. The Journal of the American Medical Association 285:1059-1070.
2. Greenfield RA, Brown BR, Hutchins JB, Iandolo JJ, Jackson R, Slater LN, Bronze MS. 2002. Microbiological, biological, and chemical weapons of warfare and terrorism. Am J Med Sci 323:326-40.
3. Wein LM, Liu Y. 2005. Analyzing a bioterror attack on the food supply: the case of botulinum toxin in milk. Proc Natl Acad Sci U S A 102:9984-9.
4. Pirazzini M, Rossetto O, Eleopra R, Montecucco C. 2017. Botulinum Neurotoxins: Biology, Pharmacology, and Toxicology. Pharmacol Rev 69:200-35.
5. Singh BR. 2006. Botulinum neurotoxin structure, engineering, and novel cellular trafficking and targeting. Neurotox Res 9:73-92.
6. Greenfield RA, Bronze MS. 2004. Current therapy and the development of therapeutic options for the treatment of diseases due to bacterial agents of potential biowarfare and bioterrorism. Curr Opin Investig Drugs 5:135-40.
7. Cherington M. 1998. Clinical spectrum of botulism. Muscle Nerve 21:701-10.
8. Simpson L. 2013. The life history of a botulinum toxin molecule. Toxicon 68:40-59.
9. Sugiyama H. 1980. Clostridium botulinum neurotoxin. Microbiol Rev 44:419-48.
10. Schiavo G, Matteoli M, Montecucco C. 2000. Neurotoxins affecting neuroexocytosis. Physiol Rev 80:717-66.
11. Lacy DB, Tepp W, Cohen AC, DasGupta BR, Stevens RC. 1998. Crystal structure of botulinum neurotoxin type A and implications for toxicity. Nat Struct Biol 5:898-902.
12. Winner BM, Bodt SML, McNutt PM. 2020. Special Delivery: Potential Mechanisms of Botulinum Neurotoxin Uptake and Trafficking within Motor Nerve Terminals. Int J Mol Sci 21.

13. Cai S, Lindo P, Park JB, Vasa K, Singh BR. 2010. The identification and biochemical characterization of drug-like compounds that inhibit botulinum neurotoxin serotype A endopeptidase activity. Toxicon 55:818-26.
14. Burnett JC, Opsenica D, Sriraghavan K, Panchal RG, Ruthel G, Hermone AR, Nguyen TL, Kenny TA, Lane DJ, McGrath CF, Schmidt JJ, Vennerstrom JL, Gussio R, Solaja BA, Bavari S. 2007. A refined pharmacophore identifies potent 4-amino-7-chloroquinoline-based inhibitors of the botulinum neurotoxin serotype A metalloprotease. J Med Chem 50:2127-36.
15. Burnett JC, Ruthel G, Stegmann CM, Panchal RG, Nguyen TL, Hermone AR, Stafford RG, Lane DJ, Kenny TA, McGrath CF, Wipf P, Stahl AM, Schmidt JJ, Gussio R, Brunger AT, Bavari S. 2007. Inhibition of metalloprotease botulinum serotype A from a pseudo-peptide binding mode to a small molecule that is active in primary neurons. J Biol Chem 282:5004-14.
16. Patel K, Cai S, Singh BR. 2014. Current strategies for designing antidotes against botulinum neurotoxins. Expert Opin Drug Discov 9:319-33.
17. Deshpande SS, Sheridan RE, Adler M. 1995. A study of zinc-dependent metalloendopeptidase inhibitors as pharmacological antagonists in botulinum neurotoxin poisoning. Toxicon 33:551-7.
18. Adler M, Nicholson JD, Starks DF, Kane CT, Cornille F, Hackley BE, Jr. 1999. Evaluation of phosphoramidon and three synthetic phosphonates for inhibition of botulinum neurotoxin B catalytic activity. J Appl Toxicol 19 Suppl 1:S5-S11.
19. Eubanks LM, Silhar P, Salzameda NT, Zakhari JS, Xiaochuan F, Barbieri JT, Shoemaker CB, Hixon MS, Janda KD. 2010. Identification of a Natural Product Antagonist against the Botulinum Neurotoxin Light Chain Protease. ACS Med Chem Lett 1:268-272.
20. Bremer PT, Adler M, Phung CH, Singh AK, Janda KD. 2017. Newly Designed Quinolinol Inhibitors Mitigate the Effects of Botulinum Neurotoxin A in Enzymatic, Cell-Based, and ex Vivo Assays. J Med Chem doi:10.1021/acs.jmedchem.6b01393.
21. Roxas-Duncan V, Enyedy I, Montgomery VA, Eccard VS, Carrington MA, Lai H, Gul N, Yang DC, Smith LA. 2009. Identification and biochemical characterization of small-molecule inhibitors of Clostridium botulinum neurotoxin serotype A. Antimicrob Agents Chemother 53:3478-86.
22. Eubanks LM, Hixon MS, Jin W, Hong S, Clancy CM, Tepp WH, Baldwin MR, Malizio CJ, Goodnough MC, Barbieri JT, Johnson EA, Boger DL, Dickerson TJ, Janda KD. 2007. An in vitro and in vivo disconnect uncovered through high-throughput identification of botulinum neurotoxin A antagonists. Proc Natl Acad Sci U S A 104:2602-7.
23. Zuniga JE, Schmidt JJ, Fenn T, Burnett JC, Arac D, Gussio R, Stafford RG, Badie SS, Bavari S, Brunger AT. 2008. A potent peptidomimetic inhibitor of botulinum neurotoxin serotype A has a very different conformation than SNAP-25 substrate. Structure 16:1588-97.
24. Rao BG. 2005. Recent developments in the design of specific Matrix Metalloproteinase inhibitors aided by structural and computational studies. Curr Pharm Des 11:295-322.
25. Suzuki T, Miyata N. 2005. Non-hydroxamate histone deacetylase inhibitors. Curr Med Chem 12:2867-80.
26. Patel KB, Cai S, Adler M, Singh BK, Parmar VS, Singh BR. 2018. Natural Compounds and their Analogues as Potent Antidotes against the Most Poisonous Bacterial toxin. Appl Environ Microbiol doi:10.1128/aem.01280-18.
27. Li L, Singh BR. 1999. High-level expression, purification, and characterization of recombinant type A botulinum neurotoxin light chain. Protein Expr Purif 17:339-44.
28. Chang TW, Blank M, Janardhanan P, Singh BR, Mello C, Blind M, Cai S. 2010. In vitro selection of RNA aptamers that inhibit the activity of type A botulinum neurotoxin. Biochem Biophys Res Commun 396:854-60.
29. Leatherbarrow RJ. 1990. Using linear and non-linear regression to fit biochemical data. Trends Biochem Sci 15:455-8.

30. Lakowicz JR. 2006. Principles of Fluorescence Spectroscopy, 3rd edition doi:10.1007/978-0-387-46312-4.
31. Humphrey W, Dalke A, Schulten K. 1996. VMD: visual molecular dynamics. J Mol Graph 14:33-8, 27-8.
32. Brooks BR, Brooks CL, 3rd, Mackerell AD, Jr., Nilsson L, Petrella RJ, Roux B, Won Y, Archontis G, Bartels C, Boresch S, Caflisch A, Caves L, Cui Q, Dinner AR, Feig M, Fischer S, Gao J, Hodoscek M, Im W, Kuczera K, Lazaridis T, Ma J, Ovchinnikov V, Paci E, Pastor RW, Post CB, Pu JZ, Schaefer M, Tidor B, Venable RM, Woodcock HL, Wu X, Yang W, York DM, Karplus M. 2009. CHARMM: the biomolecular simulation program. J Comput Chem 30:1545-614.
33. Ferrara P, Apostolakis J, Caflisch A. 2002. Evaluation of a fast implicit solvent model for molecular dynamics simulations. Proteins 46:24-33.
34. Zhmurov A, Kononova O, Litvinov RI, Dima RI, Barsegov V, Weisel JW. 2012. Mechanical transition from alpha-helical coiled coils to beta-sheets in fibrin(ogen). J Am Chem Soc 134:20396-402.
35. D.A. Case IYB-S, S.R. Brozell, D.S. Cerutti, T.E. Cheatham, III, V.W.D. Cruzeiro, T.A. Darden, R.E. Duke, D. Ghoreishi, M.K. Gilson, H. Gohlke, A.W. Goetz, D. Greene, R Harris, N. Homeyer, S. Izadi, A. Kovalenko, T. Kurtzman, T.S. Lee, S. LeGrand, P. Li, C. Lin, J. Liu, T. Luchko, R. Luo, D.J. Mermelstein, K.M. Merz, Y. Miao, G. Monard, C. Nguyen, H. Nguyen, I. Omelyan, A. Onufriev, F. Pan, R. Qi, D.R. Roe, A. Roitberg, C. Sagui, S. Schott-Verdugo, J. Shen, C.L. Simmerling, J. Smith, R. Salomon-Ferrer, J. Swails, R.C. Walker, J. Wang, H. Wei, R.M. Wolf, X. Wu, L. Xiao, D.M. York and P.A. Kollman 2018. Amber 2018.
36. Ponder JW, Case DA. 2003. Force fields for protein simulations. Adv Protein Chem 66:27-85.
37. Wang J, Wolf RM, Caldwell JW, Kollman PA, Case DA. 2004. Development and testing of a general amber force field. J Comput Chem 25:1157-74.
38. Gotz AW, Williamson MJ, Xu D, Poole D, Le Grand S, Walker RC. 2012. Routine Microsecond Molecular Dynamics Simulations with AMBER on GPUs. 1. Generalized Born. J Chem Theory Comput 8:1542-1555.
39. Salomon-Ferrer R, Gotz AW, Poole D, Le Grand S, Walker RC. 2013. Routine Microsecond Molecular Dynamics Simulations with AMBER on GPUs. 2. Explicit Solvent Particle Mesh Ewald. J Chem Theory Comput 9:3878-88.
40. Singh BR, DasGupta BR. 1989. Structure of heavy and light chain subunits of type A botulinum neurotoxin analyzed by circular dichroism and fluorescence measurements. Mol Cell Biochem 85:67-73.
41. Li L, Singh BR. 2000. Spectroscopic analysis of pH-induced changes in the molecular features of type A botulinum neurotoxin light chain. Biochemistry 39:6466-74.
42. Ware WR. 1962. OXYGEN QUENCHING OF FLUORESCENCE IN SOLUTION: AN EXPERIMENTAL STUDY OF THE DIFFUSION PROCESS. The Journal of Physical Chemistry 66:455-458.
43. Minnow YV, Goldberg R, Tummalapalli SR, Rotella DP, Goodey NM. 2017. Mechanism of inhibition of botulinum neurotoxin type A light chain by two quinolinol compounds. Arch Biochem Biophys 618:15-22.
44. Lai H, Feng M, Roxas-Duncan V, Dakshanamurthy S, Smith LA, Yang DC. 2009. Quinolinol and peptide inhibitors of zinc protease in botulinum neurotoxin A: effects of zinc ion and peptides on inhibition. Arch Biochem Biophys 491:75-84.
45. Breidenbach MA, Brunger AT. 2004. Substrate recognition strategy for botulinum neurotoxin serotype A. Nature 432:925-9.
46. Breidenbach MA, Brunger AT. 2005. New insights into clostridial neurotoxin-SNARE interactions. Trends Mol Med 11:377-81.

47. Felturp TM. 2016. Analysis of molecular topography and functional activities to decode unique features of botulinum neurotoxin endopeptidase. Ph. D. University of Massachusetts Lowell.
48. Kumar R, Kukreja RV, Li L, Zhmurov A, Kononova O, Cai S, Ahmed SA, Barsegov V, Singh BR. 2014. Botulinum neurotoxin: unique folding of enzyme domain of the most-poisonous poison. J Biomol Struct Dyn 32:804-15.
49. Litvinov RI, Kononova O, Zhmurov A, Marx KA, Barsegov V, Thirumalai D, Weisel JW. 2018. Regulatory element in fibrin triggers tension-activated transition from catch to slip bonds. Proc Natl Acad Sci U S A 115:8575-8580.
50. Kononova O, Litvinov RI, Blokhin DS, Klochkov VV, Weisel JW, Bennett JS, Barsegov V. 2017. Mechanistic Basis for the Binding of RGD- and AGDV-Peptides to the Platelet Integrin alphaIIbbeta3. Biochemistry 56:1932-1942.
51. Kononova O, Litvinov RI, Zhmurov A, Alekseenko A, Cheng CH, Agarwal S, Marx KA, Weisel JW, Barsegov V. 2013. Molecular mechanisms, thermodynamics, and dissociation kinetics of knob-hole interactions in fibrin. J Biol Chem 288:22681-92.
52. Hu X, Legler PM, Southall N, Maloney DJ, Simeonov A, Jadhav A. 2014. Structural insight into exosite binding and discovery of novel exosite inhibitors of botulinum neurotoxin serotype A through in silico screening. J Comput Aided Mol Des 28:765-78.
53. Kumar G, Kumaran D, Ahmed SA, Swaminathan S. 2012. Peptide inhibitors of botulinum neurotoxin serotype A: design, inhibition, cocrystal structures, structure-activity relationship and pharmacophore modeling. Acta Crystallogr D Biol Crystallogr 68:511-20.
54. Burnett JC, Schmidt JJ, McGrath CF, Nguyen TL, Hermone AR, Panchal RG, Vennerstrom JL, Kodukula K, Zaharevitz DW, Gussio R, Bavari S. 2005. Conformational sampling of the botulinum neurotoxin serotype A light chain: implications for inhibitor binding. Bioorg Med Chem 13:333-41.
55. Chang S, He HQ, Shen L, Wan H. 2015. Understanding peptide competitive inhibition of botulinum neurotoxin a binding to SV2 protein via molecular dynamics simulations. Biopolymers 103:597-608.